Earth's Future

Supporting Information for:

Water Sustainability, Drought, Relic Groundwater and Lithium Resource Extraction in an Arid Landscape

B. J. Moran[1] 0000-0002-9862-6241, D. F. Boutt[1] 0000-0003-1397-0279, S. V. McKnight[1] 0000-0002-6013-193X, J. Jenckes[2] 0000-0002-1811-3076, L. A. Munk[2] 0000-0003-2850-545X, Daniel Corkan[1] 0000-0001-6168-8281, Alexander Kirshen[1] 0000-0003-2015-4085

[1]Department of Geosciences, University of Massachusetts Amherst

[2]Department of Geological Sciences, University of Alaska Anchorage

Corresponding author: Brendan Moran, bmoran@geo.umass

Contents of this file

Text S1
Text S2
Text S3
Table S1
Table S2
Figure S1
Figure S2
Figure S3
Figure S4

Introduction

The supporting information contained in this section includes additional details on the methodologies used in this work including analytical methods description, assessment of remotely sensed data, and detailed descriptions of water budget calculations and groundwater level changes.

Text S1. Expanded Methods

Expanded Remotely Sensed Data Collection Methods

The JRC imagery dataset is constructed using Landsat imagery compiled from 1984 through 2020; we accessed and extracted these data using Google Earth Engine (GEE) (Gorelick et al., 2017). The JRC imagery defines each pixel as either containing water or not containing water. We defined a polygon that encompassed the Region of Interest (ROI); these ROIs were then used to clip the JRC dataset. To create a time series of monthly water extents we looped through the JRC Monthly Water History and summed the number of pixels within the ROI that were categorized as water. The pixels were then summed into a geographic area using a set of off-the-shelf functions provided by the GEE API.

To assess changes in vegetation cover we utilized the Normalized Difference Vegetation Index (NDVI) which is calculated from spectral imagery using the formula:

$$NDVI = \frac{NIR - RED}{NIR + RED}$$

where NIR is the reflection in the near-infrared spectrum and RED is the reflection in the red range of the spectrum (Tucker, 1979). NDVI is designed to assess the density of vegetation at a given location at a given time. It provides a single band with a range of -1.0 to 1.0 where negative values are clouds, water, and snow; values close to 0 up to 0.1 are rocks and bare soil. Different types of vegetation are classified in values greater than ~0.1. In this case, to be conservative and to be sure we are assessing only living vegetation (not water, soil, or potential errors at the upper boundary of the index) we extracted the pixels whose values were between 0.2 and 0.9 (NASA, 2000; USGS, 2018).

Expanded Remotely Sensed Precipitation Analysis

Through an extensive analysis of available high resolution remotely sensed and gridded precipitation datasets including TRMM-3B43, GPM-IMERG, CHIRPS, ERA5, PERSIANN-CDR, and Cr2Met, we determined that TerraClimate most closely matched both the trends and magnitudes of precipitation observed at terrestrial meteorological

stations in the SdA basin and predicted the most reasonable values of precipitation in ungauged areas based on estimates of elevation-precipitation relationships (e.g. Houston, 2009; Boutt et al., 2021). As noted by Salio et al. (2015), Schween et al. (2020), and Condom et al., (2020), satellite microwave observations such as those utilized by TRMM and GPM tend to overestimate precipitation, particularly in arid areas and over complex topography where these errors can be up to two orders of magnitude. Our analysis of these products showed overestimations at terrestrial stations of generally greater than one order of magnitude. Gridded interpolation products such as CHIRPS and PERSIANN also appear to be overestimating precipitation in the region. Since these products rely on rain gauges for calibration and interpolation of infrared remotely sensed precipitation data and since all the gauges at SdA are below 3,250 m.a.s.l., large areas of this vast basin are ungauged, particularly the high elevations. As a result, it appears the issues with interpolation likely stem from misrepresentations of these ungauged areas. CHIRPS performed somewhat better than PERSIANN at estimating precipitation values at meteorological stations perhaps due to its higher resolution, however, they both consistently overestimated precipitation by a factor of 2-3. Even the Cr2Met gridded dataset produced by the Chilean Center for Climate and Resilience Research appears to systematically overestimate precipitation amounts at ground-based meteorological stations in the basin. Another recent study with data from 2016-2019 at two meteorological stations on the eastern slope of SdA at 3,060 and 4,090 m.a.s.l. recorded average annual precipitation of 122 mm and 150 mm respectively, agreeing quite well with the TerraClimate estimates (Eshel et al., 2021). Though we do observe overestimates and underestimates in the TerraClimate dataset compared to station data, the magnitude is commonly less than other products we assessed and therefore we believe it is the best basin-scale reflection of precipitation for the region available. This is also supported by recent work by Dubey et al. (2021) that outlines the strengths of this dataset.

Expanded Water Sample Analyses Method

Tritium activity in water samples was measured at the Dissolved and Noble Gas Laboratory, University of Utah. Samples were collected in 1 L HDPE bottles with

minimal headspace. In the lab, 0.5 L aliquots were distilled to remove dissolved solids. These water samples were then degassed in stainless steel flasks until <0.01% of dissolved gas remained and sealed to ingrow helium. ^{3}H concentrations were measured by helium ingrowth (Clarke et al., 1976); 6–12 weeks is typically adequate to ingrow sufficient ^{3}He from the decay of ^{3}H ($t^{1/2}$ = 12.32 yr.; Lucas & Unterweger, 2000) for analysis. ^{3}He concentrations were then measured on a MAP215-50 magnetic sector mass spectrometer using an electron multiplier to measure low abundance ^{3}He, which was directly correlated with the amount of ^{3}H decayed. Data are reported in tritium units (TU) on the date of sampling, where one TU is equivalent to one tritium atom per 10^{18} hydrogen atoms ($^{3}H/H*10^{18}$) (Kendall & Caldwell, 1998). Several duplicate analyses of the same sample were conducted to confirm important values, and the reproducibility for these samples is of the same order as the precision of the measurement. The analytical error associated with each sample is reported along with the results in Table S1.

Water samples were analyzed for $\delta^{2}H$ and $\delta^{18}O$ using wave-length scanned cavity ring-down spectroscopy (Picarro L-1102i); samples were vaporized at 120°C (150°C for higher salt content waters) in the Stable Isotope Laboratory at the University of Alaska – Anchorage. International reference standards (IAEA, Vienna, Austria) were used to calibrate the instrument to the VSMOW-VSLAP scale and working standards (USGS45: $\delta^{2}H$ = -10.3‰, $\delta^{18}O$ = -2.24‰ and USGS46: δ2H = -235.8‰, $\delta^{18}O$ = -29.8‰) were used with each analytical run to correct for instrumental drift. Long-term mean and standard deviation records of a purified water laboratory internal QA/QC standard ($\delta^{2}H$ = -149.80‰, $\delta^{18}O$ = -19.68‰) yield an instrumental precision of 0.93‰ for $\delta^{2}H$ and 0.08‰ for $\delta^{18}O$.

Water samples analyzed for chloride compositions were filtered through 0.45 μm filters using a plastic 60 mL syringe and were stored in clean HDPE bottles. They were analyzed using a consistent, standardized procedure across two laboratories. Samples collected between 2011 and 2018 were analyzed at the University of Alaska Anchorage using an ion chromatograph (Dionex ICS 5000+) and those collected in 2021 were analyzed at the University of Massachusetts Amherst using high-pressure ion chromatography (Dionex Integrion HPIC). Waters with relatively high TDS were diluted volumetrically before analysis. Quantification was performed using seven external

calibration standards ranging from 0.1 to 100 ppb. An IonPac AS15 2×250mm column was used for anion separation using 38mM KOH as eluent and ASRS 300 zero reagent suppressor. The sample injection volume was 10 μL and quantification was performed using five external calibration standards ranging from 0 ppm to 10 ppm. Calibration verification standards and blanks were run every 10th analysis for anions. Anion analysis was verified with a secondary anion standard (Anion II Std Dionex). Samples that exceeded the calibration by 120% were diluted and re-analyzed. A charge balance assessment of these data was also done and only samples having less than 10% error were included.

Expanded Water Use Qualification Method

The 'lithium & potash mining' category was determined using SQM and Albemarle freshwater pumping data from 2014, as they are the only lithium companies using freshwater in the basin. We calculated the 'other mining' category using 2014 Minera Escondida Limitada and Compania Minera Zaldivar data. The total allocated freshwater for these two companies based on the DGA database is 2,148.7 L·s-1. Of that allocation, 1,493 L·s-1 was used in 2014, which is a ratio of 0.69. We further differentiate lithium & potash mining from other mining activities given the history of copper mining in the basin. Additional 'other mining' permits comprise 22.8 L·s-1. Because no pumping data is available for these users, the above ratio of 0.69 was applied to these allocations for an estimated actual use of 15.8 L·s-1. The only exceptions to this estimate are four concessions currently owned by the Wealth Minerals company, which are in the northern area of the salar and which, as confirmed through local experts, have never been utilized; thus, we negated the estimated use for those allocations (600 L·s-1). We rely on previous estimations of non-industrial freshwater use reported by DGA because of their relatively undocumented activities. The most recent estimates for actual use of allocated water extraction for domestic, tourism, and agricultural use are 75%, 75%, and 40%, respectively.

Text S2. Water Budget Calculations

We compare water budgets from two primary sources, the water budget currently in use by the DGA to manage water use within the SdA basin (DGA, 2013), and a revised conceptualization of the water budget (Boutt et al., 2021). We then incorporate anthropogenic water use estimates from this study into these water budgets. In the DGA water budget (Figure 9a), Precipitation (P) and Evapotranspiration from the salar (E_s) estimates are derived from DGA calculations (DGA, 2013). Based on stable isotope analyses (Godfrey et al., 2003), surface water flux (SW) and groundwater flux (GW) is estimated to be 1/3 and 2/3 of E_s, respectively. In the revised water budget (Figure 9c), P, P recharge to SW and GW, net storage flux (S), and E_s are from the most current understanding of the water budget for the basin (Boutt et al., 2021). For both the DGA and revised water budgets, the remainder of P that does not become modern recharge is assumed to become infiltration losses due to evaporation (E_i).

In the post-development scenarios for both the DGA (Figure 9b) and revised (Figure 9d) conceptualizations, anthropogenic freshwater withdrawals (W_f) and brine withdrawals (W_b) are applied to the water budget. The W_f flux from SW and GW is the estimated actual freshwater use in 2014, presented in Section 4.2 and Figure 4. We assume that any diversion of SW or GW flux to W_f results in an equal decrease in SW or GW flux to E_s, and the E_s is reduced accordingly for both post-development scenarios. We assume that all W_b flux results in a corresponding net storage flux from the brine body (S_b).

Text S3. Groundwater Storage Changes

We compiled groundwater level measurements from the SQM environmental monitoring database, Comité de Minería No Metálica CORFO (AMPHOS21, 2018), and Minera Escondida Ltda (MEL, 2017) to establish a record of groundwater level measurements from 94 monitoring points collected between September 1986 and March 2021. For each of the monitoring points, we performed a seasonal Mann-Kendall trend analysis (Hirsch et al., 1982) using pyMannKendall (Hussain et al., 2019) to assess groundwater levels from December 2007 through December 2016. This represents the longest period of continuous groundwater level records for the 94 monitoring points. We used the seasonal Sen's slope (Hipel & McLeod 1994) for the seasonal Mann-Kendall

trend to estimate the mean change in groundwater elevation for the period from December 2007 through December 2016 at each well. We then grouped the wells by the major SdA basin watershed zones (Munk et al., 2018), specified as Diffuse North East gw (n=7), Diffuse North Tumisa gw (n=16), Diffuse South Tumisa gw (n=3), Peine (n=1), and Monturaqui/Negrillar/Tilopozo (MNT) (n=8). In addition, wells located in the salar nucleus were grouped into the West Nucleus (n=24) and East Nucleus (n=35), separated by approximate location of the salar fault system (Jordan et al., 2007, Rubilar et al., 2018). We then calculated the geometric mean of the hydraulic head changes within each zone to estimate the mean for the whole watershed or nucleus zone. Using the mean change in hydraulic head estimates, we calculated the change in groundwater storage for each watershed or nucleus zone assuming a specific yield of 0.25 and using the geodesic area of the zone.

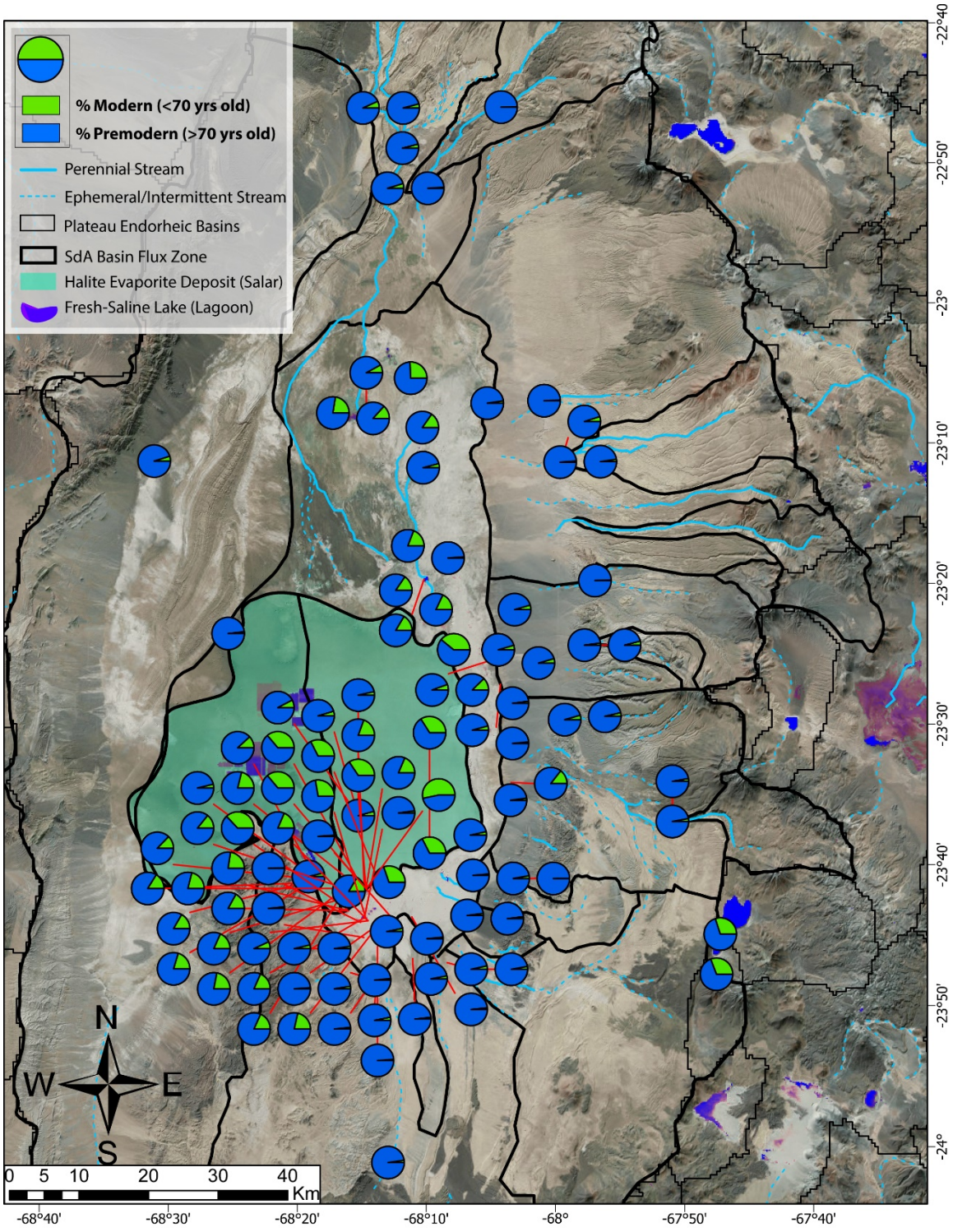

Figure S1. The percent modern water content of all samples presented in this work (n=106). Each circle represents one sample.

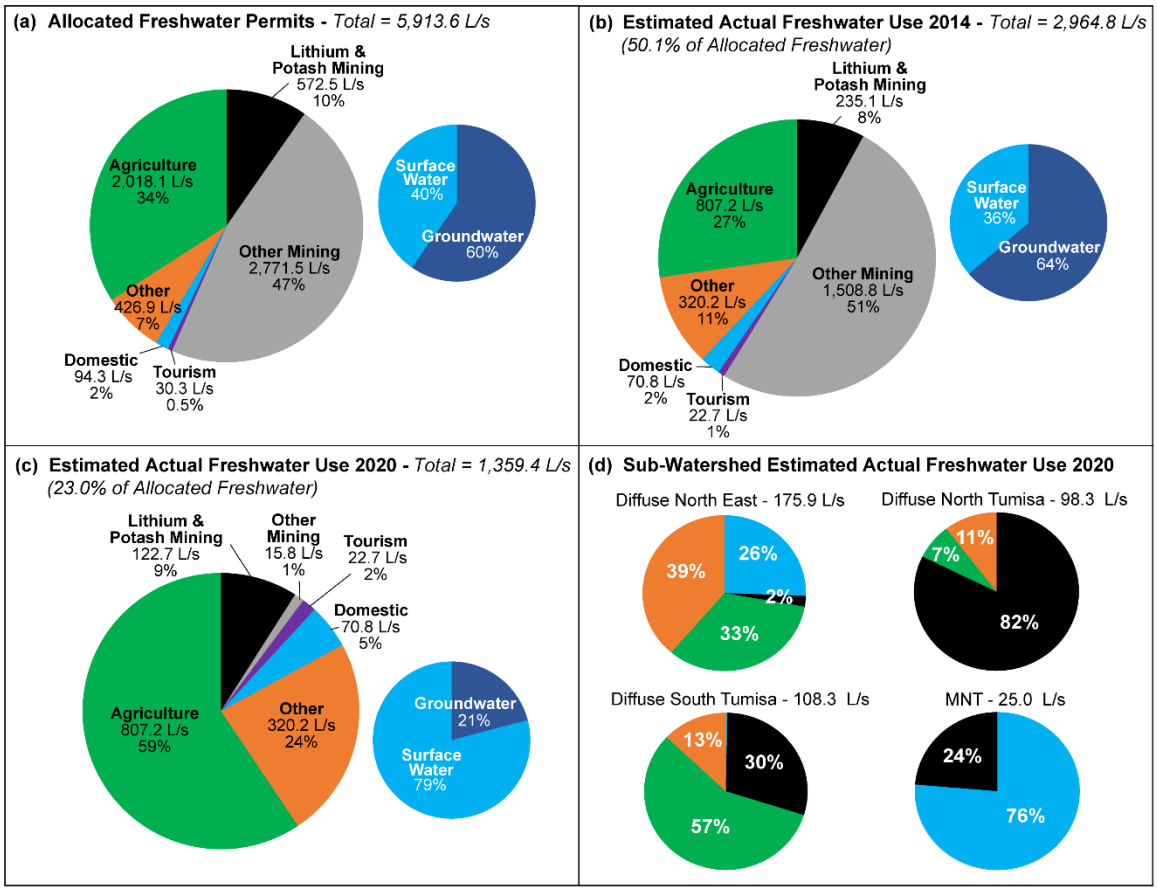

Figure S2. Pie charts of allocated freshwater permits (a); estimated actual freshwater use from 2014 (b); and estimated actual freshwater use from 2020 (c). With additional pie charts representing the percent of surface water (light blue) and groundwater (dark blue). Pie charts in (d) show estimated actual freshwater use from 2020 (L/s) within each sub-watershed zone divided by water use type: lithium mining (black), other mining (grey), agriculture (green), domestic (blue), tourism (purple), and other (orange). Percentages under 1% are not included.

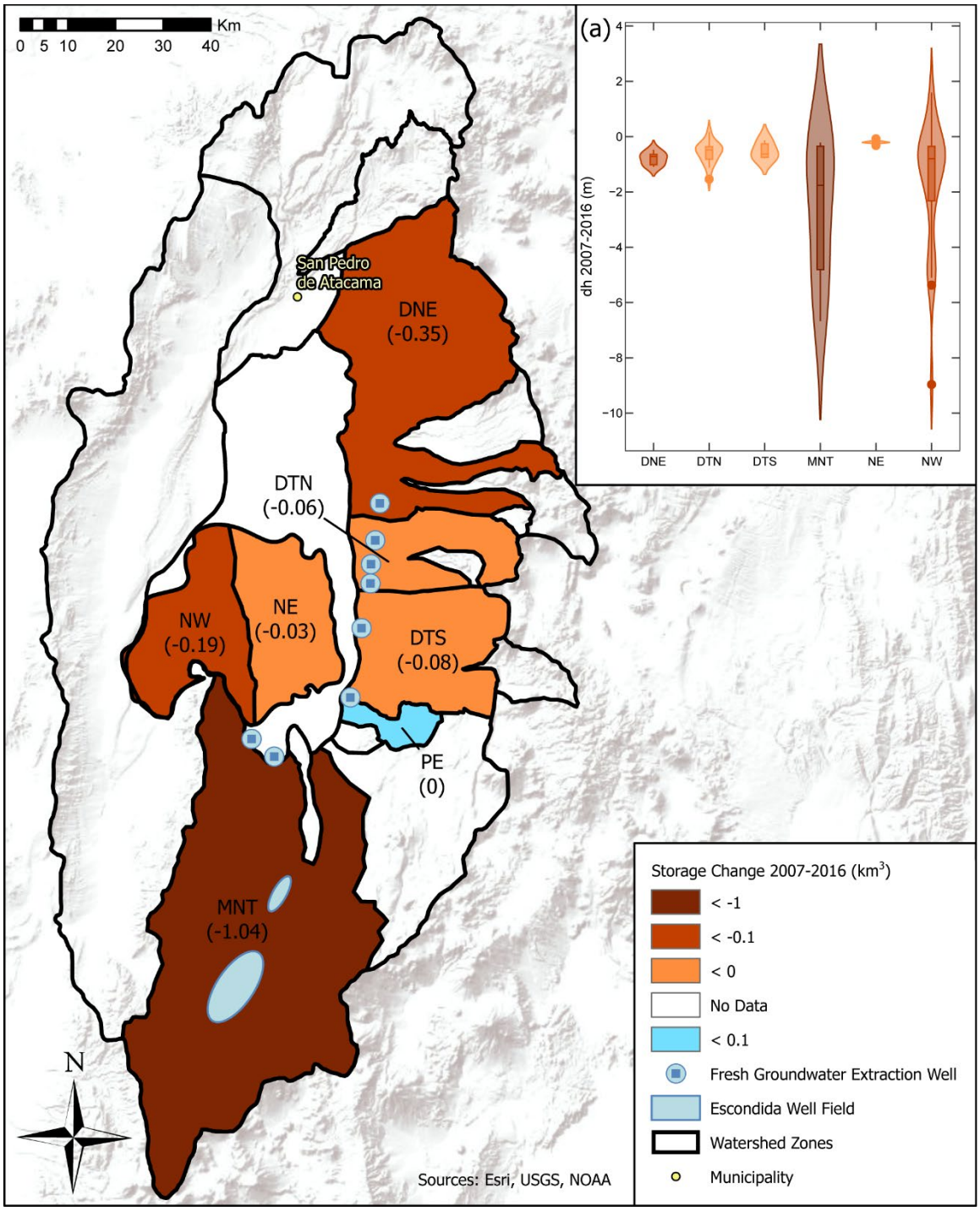

Figure S3. Estimated change in groundwater storage for watershed zones Diffuse North East gw (DNE), Diffuse North Tumisa gw (DTN), Diffuse South Tumisa gw (DTS), Peine (PE), and MNT, as well as nucleus zones East Nucleus (NE) and West Nucleus (NW) in the SdA basin. (a) Violin plot showing the distribution of mean change in the hydraulic head (dh) for monitoring wells located in each watershed or nucleus zone. The method used to obtain these results is provided in **Text S3**.

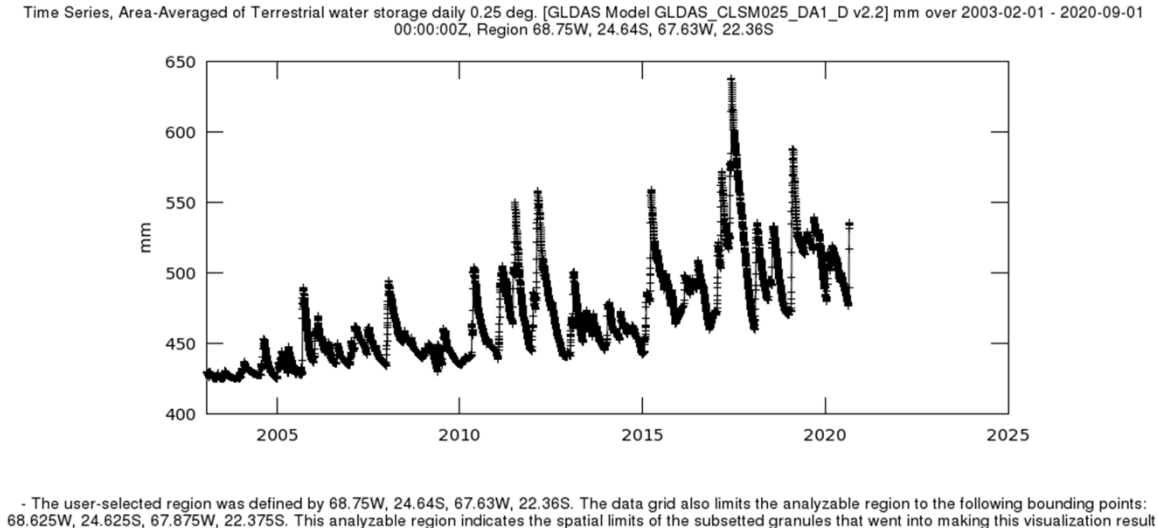

Figure S4. GLDAS v2.2 Land Surface Model output for daily terrestrial water storage change in the Salar de Atacama basin to compare with analysis by Liu & Agusdinata (2020).

Table S1. Summary of geochemical data and results used in this work.

Table S2. Piston-flow physical transit model calculations and results to compare with ^{3}H tracer-based observations of transit times.